Mitigation of plasma-wall interactions with low-Z powders in DIII-D high confinement plasmas

F. Effenberg[1], A. Bortolon[1], L. Casali[2], R. Nazikian[3], I. Bykov[3], F. Scotti[4], H.Q. Wang[3], M.E. Fenstermacher[4], R. Lunsford[1], A. Nagy[1], B.A. Grierson[3], F. M. Laggner[1], R. Maingi[1], and the DIII-D Team

1 - Princeton Plasma Physics Laboratory, Princeton, NJ 08543, USA
2 - University of Tennessee, Knoxville, TN 37996, USA
3 - General Atomics, San Diego, CA 92186, USA
4 - Lawrence Livermore National Laboratory, Livermore, CA 94550, USA

E-mail: `feffenbe@pppl.gov`

Abstract. Experiments with low-Z powder injection in DIII-D high confinement discharges demonstrated increased divertor dissipation and detachment while maintaining good core energy confinement. Lithium (Li), boron (B), and boron nitride (BN) powders were injected in H-mode plasmas (I_p =1 MA, B_t =2 T, P_{NB} =6 MW, $\langle n_e \rangle = 3.6 - 5.0 \cdot 10^{19}$ m^{-3}) into the upper small-angle slot (SAS) divertor for 2-s intervals at constant rates of 3-204 mg/s.

The multi-species BN powders at a rate of 54 mg/s showed the most substantial increase in divertor neutral compression by more than an order of magnitude and lasting detachment with minor degradation of the stored magnetic energy W_{mhd} by 5%. Rates of 204 mg/s of boron nitride powder further reduce ELM-fluxes on the divertor but also cause a drop in confinement performance by 24% due to the onset of an $n = 2$ tearing mode.

The application of powders also showed a substantial improvement of wall conditions manifesting in reduced wall fueling source and intrinsic carbon and oxygen content in response to the cumulative injection of non-recycling materials.

The results suggest that low-Z powder injection, including mixed element compounds, is a promising new core-edge compatible technique that simultaneously enables divertor detachment and improves wall conditions during high confinement operation.

Keywords: divertor power exhaust, dust injection, wall conditioning, detachment, powder injection, impurity seeding, core-edge integration

1. Introduction

Present plasma-facing component (PFCs) materials cannot withstand continuous heat fluxes above 10 MW/m^2 predicted for the next step large-scale fusion reactors such as ITER [1] or a projected future US fusion pilot plant [2]. Dissipation and spreading of heat fluxes by isotropic low-Z impurity line emission are promising techniques to prevent melting and damage and extend the lifetime of the exposed wall materials.

Usually, low-Z impurities are injected in gaseous form to enhance divertor radiation or create a radiative mantle surrounding the hot core plasma [3]. Impurity gas seeding has been developed for this purpose and extensively investigated, e.g., at the tokamaks TEXTOR, JET, Alcator C-Mod, ASDEX Upgrade, DIII-D, EAST, the heliotron LHD, and more recently at the stellarator W7-X [4, 3, 5, 6, 7, 8, 9, 10].

The radiative mantle and divertor dissipation approach prevent damage and wear of main plasma-facing components to enable safe long-pulse operation. However, the ideal solution must be core-edge compatible, i.e., power losses in the boundary and divertor plasma must not have a detrimental impact on the high-performance core plasma.

The radiative power losses by low-Z impurities reduce the temperature and sputtering in the divertor. Plasma recombination sets on at temperatures below 1 eV and creates a protective neutral gas cushion in front of the targets, protecting against incoming heat and particle fluxes. In such a regime, the plasma boundary is removed from the divertor targets, and erosion and sputtering processes are substantially suppressed. This state is called plasma detachment [11, 12].

Nitrogen and neon gases are widely used for effective power dissipation in the plasma boundary. However, nitrogen is of concern in a reactor environment due to the production of tritiated ammonia (NT3), which contaminate the uranium beds of the ITER tritium plant [13, 14]. The choice of impurities is eventually determined by their radiation characteristics and may be limited by chemistry [15, 16].

Numerical studies have suggested that alternative impurities such as boron (B) deserve consideration for radiative dissipation as well [17, 18]. However, boron delivery in gaseous form requires toxic or explosive gases like diborane (B_2D_6) or strongly diluted compounds such as trimethyl borane (C_3D_9B).

Lithium is strongly considered a liquid metal wall candidate, potentially allowing to spread and conduct heat efficiently and safely away [19, 20, 21]. Studies also predict it to be an effective dissipator in the lithium vapor box divertor [22, 23].

More recently, the injection of low-Z solid materials in powder, dust, or small granule form was introduced as a novel technique for various real-time applications. First applications focused on real-time wall conditioning, disruption mitigation, mitigation of edge localized modes (ELMs), and confinement improvement with boron, boron nitride (BN), and lithium powders at TFTR, T-10, DIII-D, EAST, ASDEX Upgrade, KSTAR, LHD, and W7-X [24, 25, 26, 27, 28, 29, 30, 31, 32, 33]. Real-time injection of powders has been particularly beneficial for long-pulse operation and at experiments using superconducting coils, where it can supplement or even substitute conventional glow discharge boronization. Low Z material injection is also being considered a method for replenishing wall claddings and surface conditioning in fusion pilot plants [34].

In the following, first-time experiments at DIII-D are presented that show strong divertor dissipation and mitigation of plasma-wall interactions during H-mode by injecting lithium, boron, and boron nitride powders into the upper closed small angle slot divertor.

The remainder of this paper is organized as follows: Section 2 provides an overview of the experiment and method of impurity injection; sections 3 and 4 present the effect of lithium, boron, and boron nitride injection on confined and divertor plasma; section 5 illustrates the beneficial effect of real-time low-recycling powder injection on wall-conditions; section 6 discusses the results in the context of recent studies; the final section 7 provides a summary.
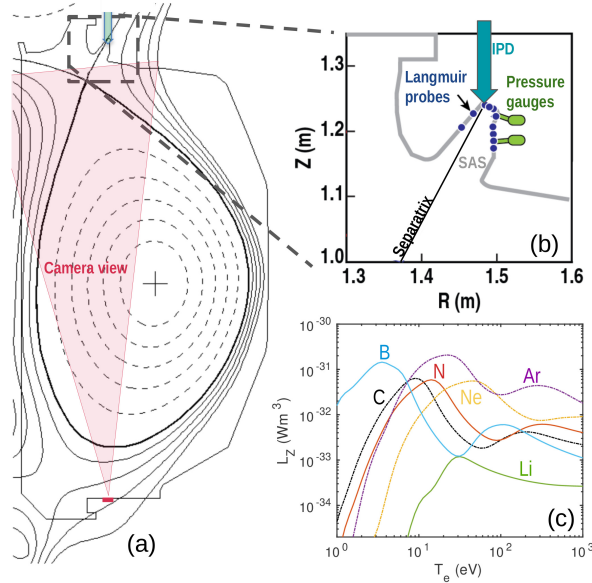
Figure 1. (a) Magnetic equilibrium and of upper single null H-mode scenarios. The arrow indicates the powder injection location in the small-angle slot divertor (SAS). (b) Langmuir probes and pressure gauges, impurity powder dropping location in the SAS divertor. (c) Power loss function $L_Z = L_Z(T_e, n_e\tau)$ for lithium, boron, carbon, nitrogen, neon, and argon in non-coronal equilibrium for $n_e\tau = 10^{20}$ m^{-3}ms.

2. Setup of low-Z powder injection in DIII-D high confinement plasmas

The experiments were conducted in upper-single null ELMy H-mode in standard and reversed toroidal field (B_t) direction $(I_p = 1.0$ MA, $B_t = 2$ T, $P_{NB} = 6$ MW, $\beta_n = 2.0$, $f_{ELM} = 80$ Hz, $n_e = 3.6 - 5.0 \cdot 10^{19}$ m^{-3}). The outer strike point (OSP) is positioned in the small-angle slot divertor. In this configuration, the ion grad-B $(B \times \nabla B)$ drift direction points away from (into) the SAS divertor in case of standard (reversed) toroidal B_t direction. Figure 1(a) shows the magnetic equilibrium, the location of the OSP at the SAS target, the powder injection location (green arrow), and the vertical camera view (DiMES TV [35]). The SAS geometry, the array of Langmuir probes (LP), the position of pressure gauges (PG), and the injection location of the impurity powder dropper (IPD) are shown in figure 1(b) in more detail. The divertor Langmuir probes and pressure gauge are used to characterize the divertor plasma. Vertical and tangential camera diagnostics measure visible and filtered line integrated brightness of different charge states of injected impurities [36, 35]. The Multi-chord Divertor Spectrometer (MDS) provides additionally high-resolution spectroscopy for the divertor SOL [37].

The closed divertor geometry generally facilitates the dissipation of heat and particle fluxes due to inherently better neutral compression [38, 39, 40, 41, 42, 43].

The species-dependent cooling behavior of different elements used in dissipation experiments is usually expressed by their radiative losses $P_{loss,rad} = n_e n_Z L_Z$, which are proportional to the electron density n_e, the impurity density n_Z and the power loss function L_Z. The power loss function describes the cooling efficiency for an impurity
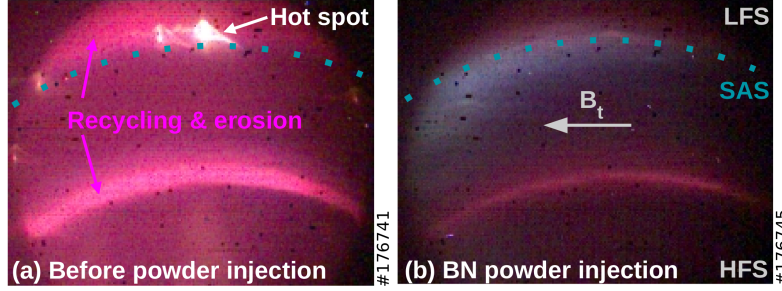
Figure 2. Vertical bottom-up view into closed divertor by visible camera (figure 1(a)) imaging (a) prior and (b) during boron nitride powder injection. The toroidal field direction (B_t), low field side (LFS), and high field side (HFS) are marked. The dashed line marks the position of the small angle slot (SAS) divertor. The bright emission belts and spots represent boundary emission from plasma-wall interactions and hot spot spots.

as a function of only the electron temperature in coronal equilibrium in the core plasma [44]. However, the plasma edge is in non-coronal equilibrium due to steep gradients, and associated transport [45]. Here, the power loss function also depends on the non-equilibrium parameter $n_e\tau$ with τ being the particle residence time: $L_Z = L_Z(T_e, n_e\tau)$. The non-equilibrium power loss function is shown in figure 1(c), assuming $n_e = 10^{20}$ m^{-3} and a particle residence time of 1 ms in the plasma edge for lithium, boron, carbon, nitrogen, neon, and argon. These elements are introduced in powder form in the present study (B, Li, BN) or are intrinsically released (C) through erosion or extrinsically injected as impurity gas (N, Ne, Ar) during conventional radiative power exhaust experiments. The total line emission has been calculated with atomic data from ADAS [46]. Boron shows for L_Z a maximum at a few eV while lithium reaches its maximum at a few tens of eV corresponding to far and near scrape-off layer (SOL) temperatures, respectively. Nitrogen shows peak radiation around 10 eV. The radiation potentials suggest that B, N, C causes power losses mainly in the SOL, while Li and Ne may radiate in the near SOL and around the separatrix. Ar shows substantial losses also at higher temperatures in the confinement. The impurity powder dropper (IPD) [47] is mounted at the top of the DIII-D tokamak device at a toroidal angle of 195°. The radial drop location is $R = 1.484$ m. It has four reservoirs filled with different types of impurity powders. Impurity powders were dropped directly into the OSP region through a tube of 2 m length into the SAS. The powder particles reach velocities of $5 - 6$ m/s upon divertor entrance due to acceleration by gravitational force. The time delay between actuation and impact on the divertor plasma with the current DIII-D setup is typically 900 ms, whereas impurity gas feedback allows response within 250-500 ms. The macroscopic powder particles must undergo ablation, which depends on the powder particle size. Lithium and boron nitride powders were of relatively fine size (up to 40 and 65 μm), while the boron powder used consists of relatively large sizes (up to 150 μm).

3. Cooling of the plasma boundary with lithium, boron and boron nitride powders

In a sequence of experiments, boron, boron nitride, and lithium were injected in powder form in H-mode (#176740-52). The low-Z powders were released into the divertor plasma at 2.9 s. Mass flow rates of 3-204 mg/s were determined with a flow meter [47] corresponding to atomic rates of $0.2 - 5.4 \cdot 10^{21} \frac{atoms}{s}$.

A bottom-up camera view (figure 1(a)) was used to capture the visible emission from plasma-wall interactions on the high field side (HFS) and low field side (LFS) plasma-facing components. The emission is shown in figure 2(a) before and (b) during BN powder injection of experiments conducted in the standard configuration with the ion grad-B drift pointing out of the upper SAS divertor. Before powder injection, bright emission was present at and near the outer and inner strike lines and the recycling regions (figure 2(a)). Also, a hot spot was detected on the low field side at a leading tile edge. The strong boundary emission at the low and high field sides results from neutral D_α and intrinsic impurities sputtered from the plasma-facing components. During injection of BN powder ($\geq$ 200 mg/s), boundary emission and hot spot were suppressed (figure 2(b)).

During experiments with lithium and boron powder injections (3-35 mg/s), components of the spatial emission distributions are captured with the tangential camera. The camera filters extract Li II at 546 nm and B II at 410 nm, which are the only proxies for the spatial distribution of B and Li radiative power losses at this point. Since D_δ and C III emit within the band-pass of the filter used to image boron emission, background emission before boron injection was subtracted from the camera images. However, some residual contamination might remain due to a change of emissivity resulting from local cooling from the injected powder. The spatial brightness distributions are shown in figure 3 for single ionized lithium (a) and boron (b) at times during the injection, i.e., 5444 ms and 4258 ms, respectively. Vertical blue and green dashed lines in figure 3(a) and (b) indicate the innermost radial extend of the B II and Li II radiation zones. The Li II radiation is concentrated along the outer divertor leg, extending from the SAS volume to the X-point. The B II emission shows stronger brightness in a layer close to the PFCs and extends in the radial direction outwards near the targets. There is almost no overlap in the spatial distributions between the Li II and B II radiation in the radial direction. The distinct features of the emission distribution of Li and B are consistent with the temperature dependency of the cooling potentials (figure 1(c)). Boron cools the SOL while lithium causes temperature reduction in the vicinity of the separatrix. Unfortunately, during these first-time experiments, matching the powder flow rates between different species was not possible due to a lack of fine control. However, the results show substantial cooling of the divertor plasma with 3.3 mg/s lithium and 35 mg/s boron powder injection. The time traces in figure 3(c-j) show a comparison of three representative H-mode plasmas with lithium, boron and boron nitride powder injections. The Li II (547 nm), B II (608 nm), and N II (399 nm) line emissivities measured with the Multi-chord Divertor Spectrometer increase when the powder reaches the plasma around 2.8-2.9 seconds (however, data for N II are missing after 3.7 seconds). The line averaged density increases only slightly by 5% during lithium injection, drops by 8% during boron injection and remains constant for BN injection. Z_{eff} remains constant in the case of Li, and nearly constant in the case of BN ($\Delta Z_{eff} \approx +3\%$) but increases from 1.8 to 2.4 during B injection. The stored magnetic energy reduces by 5% in the case of
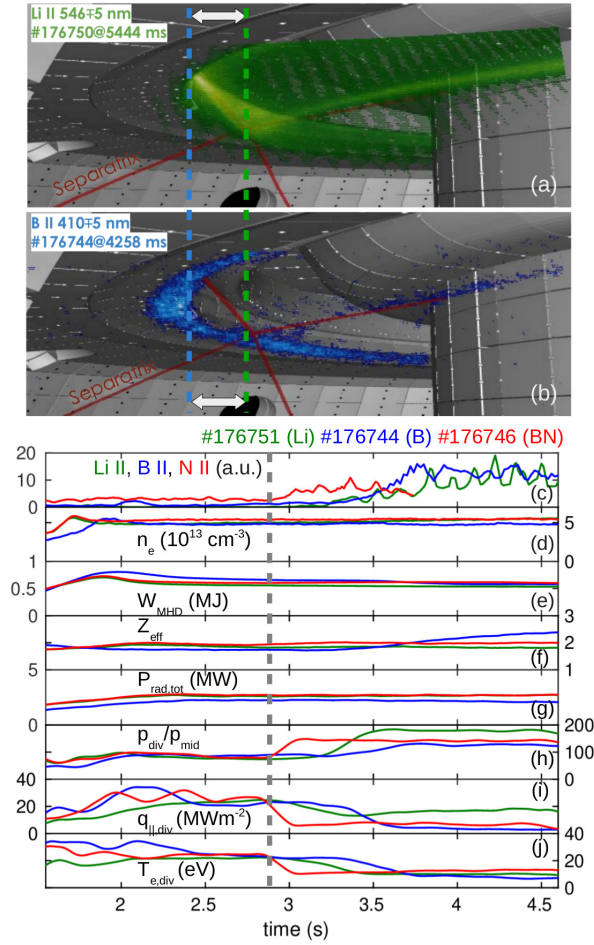
Figure 3. Line emissivities for (a) Li II (546 nm) and (b) B II (410 nm) were observed with tangential cameras. Vertical dashed lines indicate the innermost radial extend of the B II and Li II radiation zones. Time traces of (c) divertor spectral line emissivities of Li II (546 nm), B II (608 nm) and N II (399 nm), (d) line averaged electron density, (e) stored magnetic energy W_{MHD}, (f) effective charge (Z_{eff}), (g) total radiated power $P_{rad,tot}$, (h) neutral compression (ratio of divertor-to-midplane pressure), (i) peak divertor parallel heat flux $q_{\parallel,div}$, and (j) peak divertor electron temperature $T_{e,div}$. Lithium (3.3 mg/s), boron (35 mg/s) and boron nitride (13 mg/s) powder injections start at $\approx 2.8 - 2.9$ seconds.

Li and remains unchanged during BN injection. In the case of boron injection, a rate of 35 mg/s eventually triggers a $n = 2$ tearing mode which reduces stored magnetic energy by 14% after 3.5 s. The total radiated power remains mostly stable at 2.6 MW for Li and BN and 2.2 MW for B injection. The coverage of the small angle slot divertor is insufficient for quantifying the divertor radiation. The signals from individual bolometer chords closest to the SAS divertor suggest an increase in local radiation by 15-30% during Li and B injection, which does not significantly alter the measured total radiated power $P_{rad,tot}$ (figure 3(g)). Dilution effects are estimated

by measuring the rate of neutrons produced by deuterium-deuterium collisions during neutral beam injection. The measured neutron rates are related to the expected neutron emission based on a zero-dimensional calculation that includes the carbon density as the only impurity source [48] which allows estimating the dilution effects of injected impurities. The neutron rates before powder injection are $0.8 - 1.1 \times 10^{15}$ n/s. Deuterium plasma dilution with Li and B impurities causes a drop of neutron rates by up to 10% and 25%. The divertor neutral compression shown in figure 3(h) is defined as the ratio of divertor neutral pressure to main chamber pressure (measured at the outboard midplane). The divertor neutral gas pressure increases from 0.3 mtorr to 0.9 mtorr in the case of Li but only to 0.5 mtorr in the case of B injection. The divertor neutral compression increases by a factor of 3, 1.5, and 1.8 following the lithium, boron, and boron nitride powder injections. The peak electron temperatures and peak parallel heat fluxes measured with divertor Langmuir probes are shown in figure 3(h,i) reduce substantially after powder injection. In the case of low-rate Li powder injection, the peak electron temperature and heat flux are reduced by 12 eV and 10 MW/m^2, respectively. A medium rate of B results in a reduction by 20 eV and heat flux detachment. BN caused a rapid drop in $q_{\parallel,div}$ by 75% and drop of $T_{e,div}$ from 25 eV by 15 eV within 200 ms within 200 ms. At these relatively low rates, Li enhances the particle flux and density at the peak location contributing to a partial recovery of the parallel heat flux. On the other hand, the boron and boron nitride powders also reduce the divertor particle fluxes and densities.

4. Sustained divertor detachment and strong neutral compression with boron nitride powder

Injection of boron nitride at higher rates of 54 mg/s (#176946) and above (#176945) in configurations with ion $B \times \nabla B$ drift directed into the upper SAS divertor resulted in detachment and strong neutral compression. Figure 4(a-i) shows the time traces of line averaged density, stored magnetic energy, effective charge state Z_{eff}, total radiated power, divertor neutral compression, neutral deuterium emission in the divertor D_α and the divertor peak parallel heat fluxes and electron temperatures in the divertor. Divertor heat fluxes and temperature rapidly decrease and remain suppressed during BN injection ($T_{e,div} \leq 5$ eV). The increase in divertor neutral gas compression by more than one order of magnitude means a substantial contribution to dissipation by ion-neutral friction forces in the small-angle slot divertor. The D_α emission shows that ELM-fluxes in the divertor reduce in frequency for 54 mg/s and further reduce in amplitude at a very high rate of 204 mg/s due to dissipation. The effective charge Z_{eff} increases from base level by 0.8 to 2.3 while the stored magnetic energy W_{mhd} drops from 0.7 MJ by 5% during 54 mg/s BN injection. At the high rate of 204 mg/s, energy confinement drops by 24% due to an $n = 2$ tearing mode triggered after 3.8 s and Z_{eff} increases to 4.5. The total radiated power increases by 15%, and 25%, respectively (figure 4(d)). Individual bolometer chords near the SAS divertor show a local increase in radiated power by at least 40% and 60%, respectively. Using the approach mentioned above, the rate of neutrons reduces by up to 28%-38% at higher BN powder injection rates (54-204 mg/s) due to dilution effects on the core plasma. The rate of neutrons produced during deuterium-deuterium collisions during neutral beam injection has dropped to 62% of the initial level ($8.8 \cdot 10^{14}$ n/s) at 4.5 s due to dilution effects on the core plasma during moderate and high BN injection (54-204 mg/s). However, the neutron rates (up to $1 \cdot 10^{15}$ n/s) were maintained without or with
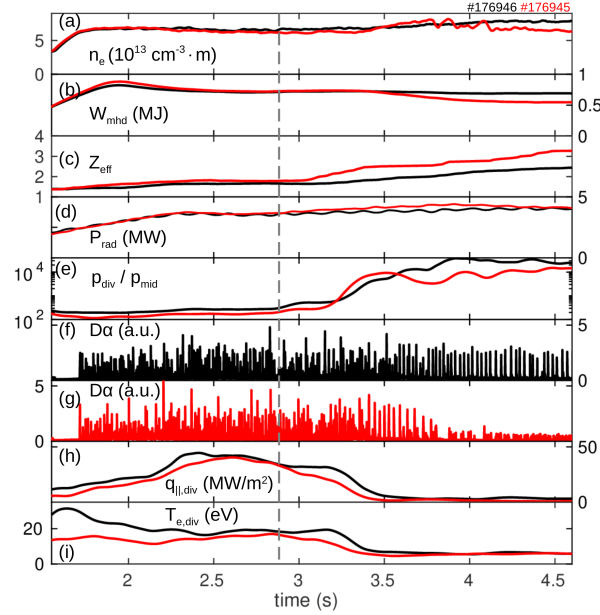
Figure 4. Time traces for boron nitride (BN) at high injection rates of 54 mg/s (black) and 204 mg/s (red). (a) line averaged electron density (b) stored magnetic energy W_{mhd}, (c) effective charge Z_{eff}, (d) total radiated power $P_{rad,tot}$, (e) divertor neutral compression, (f, g) divertor neutral emission D_α, (h) peak divertor parallel heat flux $q_{\parallel,div}$, and (i) peak divertor electron temperature $T_{e,div}$. The powder injection starts at ≈ 2.9 seconds.

only more minor losses during other scenarios with low-Z powder injection. Therefore, it is suggested that the core-edge compatibility can be optimized by modifying the injection rates and powder mix for a specific plasma scenario.

5. Improving wall conditions

Successive powder injections into the upper divertor during these experiments (#176740-51) resulted in a significant improvement of wall conditions. The strongest effects of wall conditioning were measured during the first sequence of boron powder injection experiments for which in figure 5, the time traces of (a) D_α, (b) main chamber neutral pressure p_{mid}, (c) C IV and (d) O IV are shown for the initial L-mode phase (< 1.6 s).

D_α and main chamber neutral pressure reduce after each discharge with B powder injection. The reduction in D_α emission and neutral pressure suggests a decrease of the intrinsic neutral source, i.e., wall recycling and out-gassing. Higher levels of neutral gas are injected to achieve the same target density following B injections. At the same time, CIV and OIV brightness reduce, which suggests a reduction in the intrinsic impurity source. A reduction in the impurity line emission may in parts be due to an increase in the boundary plasma temperature following a reduction in density. Unfortunately, no upstream SOL electron temperature measurements are available in this case. The wall conditioning metric C_W shown in figure 5 (e) is defined as the ratio
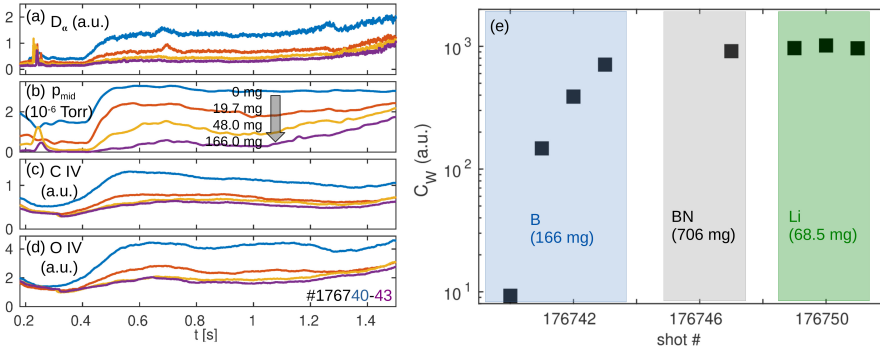
Figure 5. Change in wall conditioning before and after boron powder injection represented by time traces of (a) D_α line emission in the divertor, (b) main chamber neutral pressure p_{mid} measured at the midplane, (c) C IV (384 nm) emission, and (d) O IV (555 nm) emission during initial L-mode phase. The cumulative mass (mg) of boron powder deposited prior to each experiment is indicated. (e) Shot-by-shot change of the ratio of deuterium gas input Γ_{D2} to electron density n_e (wall conditioning metric C_W), which have been calculated as an average value over a 1.2 s time window (from $t = 0.3$ s to 1.5 s) during the initial L-mode phase. The cumulative amounts of powder are indicated in mg for each powder type.

between deuterium gas input and line averaged electron density evaluated during the L-mode phase from $t = 0.3$ s to 1.5 s: $C_W \propto \frac{\Gamma_{D2}}{n_e}$. Improving wall conditions based on this metric means reducing the intrinsic neutral source, which allows for better plasma density control through external gas input. A better density control through improved wall conditions was achieved, expressed in the ratio between gas input and density sharply increasing during the first boron injection experiments. The wall conditions dramatically improve after injection of the first 166 mg of B: $\frac{C_W(166\ mg\ B)}{C_W(0\ mg\ B)} \approx 100$. The growth rate of in-situ boron coatings on PFCs was determined to be $\approx$1 nm/s per 10 mg/s during recent DIII-D experiments [27]. Wall conditioning matures following shots with a total of 706 mg BN powder injection and does not improve further following 68.5 mg Li powder injection.

6. Discussion

Low-Z powder injection has been very suitable for reducing heat fluxes, increasing neutral build-up in the divertor, and improving wall conditions by forming low recycling coatings on the main plasma-facing components. Boron was suitable for cooling divertor heat fluxes and temperatures and showed the most significant improvement in wall conditions. However, it showed less effectiveness regarding divertor neutral compression. The neutral compression is higher and increases further with lithium and boron nitride injection. Moreover, the latter affect Z_{eff} much less than boron. 54 mg/s BN reduced divertor electron temperature below to ≤ 5 eV. Very high rates of BN (204 mg/s) also substantially reduce ELM fluxes but cause losses of 24% to W_{mhd}.

The scenarios with the ion $B \times \nabla B$ drift pointing away from the SAS require lower powder injection rates to achieve substantial cooling effects and detachment.

This is plausible since the onset of detachment also occurs at lower densities in this configuration [39].

Differences in divertor dissipation and core plasma dilution, particularly between boron and boron nitride, may be due to the different particle sizes and particle ablation. The B particles have a size up to 150 μm and can penetrate deeper into the plasma than the 65 μm BN particles. Experiments are planned to investigate the effect of particle size in comparison to modeling.

The line emission distributions obtained with tangential cameras are consistent with the temperature dependencies of the cooling potentials shown in figure 1(c) for the respective impurities. The data suggest that boron radiates at lower scrape-off layer temperatures than lithium, which may help optimize the SOL-to-core fraction in radiative losses.

Future modeling will be necessary to disentangle the effects of particle size, injection rates, radiation behavior, and potentially drift effects on the divertor plasma distribution.

Powders injected at higher rates, i.e., several tens in case of large-grained boron and several hundreds of mg/s in case of fine-grained BN, increase the risk of the onset of tearing modes. These tearing modes are detrimental to confinement and occur during radiative mantle, and radiative divertor experiments with impurity gas seeding [49].

Wall conditions improved significantly after injecting powders into the closed divertor. The substantial reduction in recycling, carbon, and oxygen levels is consistent with results reported earlier for dedicated real-time wall conditioning experiments in lower single null configurations. Experiments with low recycling materials at ASDEX-U and DIII-D have shown that conditioning of material surfaces in the private flux region, the far SOL and components such as tungsten ion-cyclotron antennas is possible [26, 50, 27, 51, 52]. ELMs and ballistic transport of neutral impurities may contribute to deposition on the main chamber wall. An essential difference in the present work is that wall conditions improve by injecting boron powder into the divertor (compared to an upstream injection location in the plasma crown). This suggests that divertor powder injection may also be beneficial for reducing high-Z impurity sources in a new tungsten divertor [53].

A general advantage of powder injection is that certain impurities can be delivered in pure form (no dilution through additional hydrogen bonding, like methane or diborane) and are not toxic or explosive. Recent studies at EAST and KSTAR show promising results regarding real-time wall conditioning in long pulse scenarios [54, 28]. Results from ASDEX-U have also shown that boron nitride powder injection reduces the ammonia content by 90% compared to nitrogen gas seeding [50]. However, fuel (tritium) retention in low recycling coatings remains a concern, and future studies will be dedicated to this topic.

In most current experiments, the delivery of solid material used a dropping technique relying on gravitational acceleration. Top powder injection facilitates dissipation in upper divertor configuration but might be less effective in lower divertor configurations. Additional devices have been developed and used for horizontal material, and powder injection, also suitable for lower divertor applications [55, 56, 57, 52]. Bottom-up injection of materials into the lower divertor has recently been demonstrated at DIII-D and will be further developed. [58].

7. Summary

Injection of boron, boron nitride, and lithium powders into the closed small angle slot (SAS) divertor during high confinement plasma operation has been found to reduce the divertor heat fluxes and improve wall conditions at the DIII-D tokamak.

Boron radiates deeper in the SOL at lower temperatures (1-10 eV) while lithium radiates at higher electron temperatures near the separatrix (10-100 eV). Boron nitride combines the dissipative properties of both boron and nitrogen and appears to be most effective for divertor power dissipation. Li and BN powders have increased neutral compression and reduced heat fluxes more effectively than B powder. Divertor detachment was achieved at a BN rate of 54 mg/s (the minimum BN flow rate for detachment might be lower). BN at rates up to 204 mg/s also suppressed ELM-fluxes to the divertor but triggered $n = 2$ tearing modes and reduced neutron rates and core energy confinement by 24%.

A total of 166 mg boron powder deposited throughout four discharges (corresponding to average rates on the order of $\approx$10 mg/s) improved the wall conditioning ratio of gas-input to electron density by a factor of $\approx$100. Low Z coatings growing on the PFCs at $\approx$1 nm/s per 10 mg/s of powders injected reduced wall recycling, carbon, and oxygen influxes.

Additional studies will be necessary to address the issue of fuel retention (tritium) and better understand the effects of particle size (44-150 μm), impurity species, and their impact on the plasma-surface interactions.

Real-time powder injection provides access to a more extensive range of impurity species for dissipative power exhaust. Optimization of the flow rates may achieve sufficient divertor dissipation while maintaining high core energy confinement. Low-Z powder injection into the divertor is a promising new approach to suppress high heat fluxes to the divertor targets and improve core-edge compatibility.

Acknowledgements

Disclaimer

not infringe privately owned rights. Reference herein to any specific commercial product, process, or service by trade name, trademark, manufacturer, or otherwise does not necessarily constitute or imply its endorsement, recommendation, or favoring by the United States Government or any agency thereof. The views and opinions of authors expressed herein do not necessarily state or reflect those of the United States Government or any agency thereof.

References

[1] R. A. Pitts, S. Carpentier, F. Escourbiac, T. Hirai, V. Komarov, S. Lisgo, A. S. Kukushkin, A. Loarte, M. Merola, A. S. Naik, R. Mitteau, M. Sugihara, B. Bazylev, P. C. Stangeby, A full tungsten divertor for ITER: Physics issues and design status, Journal of Nuclear Materials 438 (2013) S48 – S56. `doi:10.1016/j.jnucmat.2013.01.008`.

[2] National Academy of Engineering, E. National Academies of Sciences, and Medicine, Bringing Fusion to the U.S. Grid, The National Academies Press, Washington, DC, 2021. `doi:10.17226/25991`.

[3] G. Maddison, C. Giroud, G. McCormick, J. Alonso, B. Alper, G. Arnoux, P. da Silva Aresta Belo, M. Beurskens, A. Boboc, S. Brezinsek, I. Coffey, S. Devaux, T. Eich, W. Fundamenski, D. Harting, A. Huber, S. Jachmich, I. Jenkins, E. Joffrin, M. Kempenaars, M. Lehnen, T. Loarer, P. Lomas, A. Meigs, P. Morgan, V. Riccardo, F. Rimini, M. Stamp, G. Telesca, H. Thomsen, JET EFDA contributors, Moderation of divertor heat loads by fuelling and impurity seeding in well-confined ELMy H-mode plasmas on JET, Nuclear Fusion 51 (4) (2011) 042001. `doi:10.1088/0029-5515/51/4/042001`.

[4] U. Samm, G. Bertschinger, P. Bogen, J. D. Hey, E. Hintz, L. Konen, Y. T. Lie, A. Pospieszczyk, D. Rusbuldt, R. P. Schorn, B. Schweer, M. Tokar, B. Unterberg, Radiative edges under control by impurity fluxes, Plasma Physics and Controlled Fusion 35 (SB) (1993) B167–B175, publisher: IOP Publishing. `doi:10.1088/0741-3335/35/sb/013`.

[5] M. Reinke, J. Hughes, A. Loarte, D. Brunner, I. Hutchinson, B. LaBombard, J. Payne, J. Terry, Effect of N2, Ne and Ar seeding on Alcator C-Mod H-mode confinement, Journal of Nuclear Materials 415 (1, Supplement) (2011) S340–S344, Proceedings of the 19th International Conference on Plasma-Surface Interactions in Controlled Fusion. `doi:https://doi.org/10.1016/j.jnucmat.2010.10.055`.

[6] A. Kallenbach, M. Bernert, M. Beurskens, L. Casali, M. Dunne, T. Eich, L. Giannone, A. Herrmann, M. Maraschek, S. Potzel, F. Reimold, V. Rohde, J. Schweinzer, E. Viezzer, M. Wischmeier, the ASDEX Upgrade Team, Partial detachment of high power discharges in ASDEX Upgrade, Nucl. Fusion 55 (5) (2015) 053026. `doi:10.1088/0029-5515/55/5/053026`.

[7] L. Casali, T. H. Osborne, B. A. Grierson, A. G. McLean, E. T. Meier, J. Ren, M. W. Shafer, H. Wang, J. G. Watkins, Improved core-edge compatibility using impurity seeding in the small angle slot (SAS) divertor at DIII-D, Physics of Plasmas 27 (6) (2020) 062506. `doi:10.1063/1.5144693`.

[8] J. Chen, Y. Duan, Z. Yang, L. Wang, K. Wu, K. Li, F. Ding, H. Mao, J. Xu, W. Gao, L. Zhang, J. Wu, G.-N. Luo, EAST Team, Radiative divertor behavior and physics in Ar seeded plasma on EAST, Chinese Physics B 26 (9) (2017) 095205. `doi:10.1088/1674-1056/26/9/095205`.

[9] T. Morisaki, K. Oyama, N. Tamura, S. Masuzaki, T. Akiyama, G. Motojima, J. Miyazawa, B. J. Peterson, N. Ohno, H. Yamada, LHD Experiment Group, Radiated power distributions in impurity-seeded plasmas in LHD, Journal of Nuclear Materials 463 (2015) 640 – 643. `doi:10.1016/j.jnucmat.2015.01.016`.

[10] F. Effenberg, S. Brezinsek, Y. Feng, R. König, M. Krychowiak, M. Jakubowski, H. Niemann, V. Perseo, O. Schmitz, D. Zhang, T. Barbui, C. Biedermann, R. Burhenn, B. Buttenschön, G. Kocsis, A. Pavone, F. Reimold, T. Szepesi, H. Frerichs, Y. Gao, U. Hergenhahn, S. Kwak, M. Otte, T. Sunn Pedersen, W7-X Team, First demonstration of radiative power exhaust with impurity seeding in the island divertor at Wendelstein 7-X, Nuclear Fusion 59 (10) (2019) 106020. `doi:10.1088/1741-4326/ab32c4`.

[11] G. F. Matthews, Plasma detachment from divertor targets and limiters, Journal of Nuclear Materials 220-222 (1995) 104 – 116. `doi:10.1016/0022-3115(94)00450-1`.

[12] S. I. Krasheninnikov, A. S. Kukushkin, A. A. Pshenov, Divertor plasma detachment, Physics of Plasmas 23 (5) (2016) 055602. `doi:10.1063/1.4948273`.

[13] D. Neuwirth, V. Rohde, T. Schwarz-Selinger, ASDEX Upgrade Team, Formation of ammonia

during nitrogen-seeded discharges at ASDEX Upgrade, Plasma Physics and Controlled Fusion 54 (8) (2012) 085008. `doi:10.1088/0741-3335/54/8/085008`.

[14] L. Laguardia, R. Caniello, A. Cremona, G. Gatto, G. Gervasini, F. Ghezzi, G. Granucci, V. Mellera, D. Minelli, R. Negrotti, M. Pedroni, M. Realini, D. Ricci, N. Rispoli, A. Uccello, E. Vassallo, Influence of He and Ar injection on ammonia production in N2/D2 plasma in the medium flux GyM device, Nuclear Materials and Energy 12 (2017) 261–266, proceedings of the 22nd International Conference on Plasma Surface Interactions 2016, 22nd PSI. `doi:10.1016/j.nme.2017.05.009`.

[15] A. Kallenbach, M. Bernert, R. Dux, L. Casali, T. Eich, L. Giannone, A. Herrmann, R. McDermott, A. Mlynek, H. W. Müller, F. Reimold, J. Schweinzer, M. Sertoli, G. Tardini, W. Treutterer, E. Viezzer, R. Wenninger, M. Wischmeier, ASDEX Upgrade Team, Impurity seeding for tokamak power exhaust: from present devices via ITER to DEMO, Plasma Physics and Controlled Fusion 55 (12) (2013) 124041, publisher: IOP Publishing. `doi:10.1088/0741-3335/55/12/124041`.

[16] R. J. Walker, M. R. Gilbert, Neutron activation of impurity seeding gases within a DEMO environment, Fusion Engineering and Design 124 (2017) 892 – 895. `doi:10.1016/j.fusengdes.2017.01.057`.

[17] A. Y. Pigarov, Radiative detached divertor with acceptable separatrix Zeff, Physics of Plasmas 24 (10) (2017) 102521. `doi:10.1063/1.4986516`.

[18] F. Effenberg, A. Bortolon, H. Frerichs, B. Grierson, J. Lore, T. Abrams, T. Evans, Y. Feng, R. Lunsford, R. Maingi, A. Nagy, R. Nazikian, D. Orlov, J. Ren, D. Rudakov, W. Wampler, H. Wang, 3D modeling of boron transport in DIII-D L-mode wall conditioning experiments, Nuclear Materials and Energy 26 (2021) 100900. `doi:10.1016/j.nme.2021.100900`.

[19] M. Poradziński, I. Ivanova-Stanik, G. Pełka, V. P. Ridolfini, R. Zagórski, Integrated power exhaust modelling for DEMO with lithium divertor, Fusion Engineering and Design 146 (2019) 1500–1504, sI:SOFT-30. `doi:10.1016/j.fusengdes.2019.02.115`.

[20] D. Andruczyk, R. Maingi, J. S. Hu, G. Z. Zuo, R. Rizkallah, M. Parsons, A. Shone, D. O'Dea, A. Kapat, M. Szott, S. Stemmley, Z. Sun, W. Xu, X. C. Meng, R. Lunsford, E. P. Gilson, A. Diallo, K. Tritz, EAST Team, Overview of lithium injection and flowing liquid lithium results from the US-China collaboration on EAST, Physica Scripta T171 (2020) 014067. `doi:10.1088/1402-4896/ab6ce1`.

[21] E. Marenkov, A. Kukushkin, A. Pshenov, Modeling the vapor shielding of a liquid lithium divertor target using SOLPS 4.3 code, Nuclear Fusion 61 (3) (2021) 034001. `doi:10.1088/1741-4326/abd642`.

[22] R. J. Goldston, R. Myers, J. Schwartz, The lithium vapor box divertor, Phys. Scr. T167 (2016) 014017. `doi:10.1088/0031-8949/T167/1/014017`.

[23] J. A. Schwartz, E. D. Emdee, R. Goldston, M. Jaworski, Physics design for a lithium vapor box divertor experiment on Magnum-PSI, Nuclear Materials and Energy 18 (2019) 350–355. `doi:10.1016/j.nme.2019.01.024`.

[24] J. Snipes, E. Marmar, J. Terry, M. Bell, R. Budny, K. Hill, D. Jassby, D. Mansfield, D. Meade, H. Park, J. Strachan, B. Stratton, E. Synakowski, G. Taylor, D. Ruzic, M. Shaheen, TFTR Group, Wall conditioning with impurity pellet injection on TFTR, Journal of Nuclear Materials 196-198 (1992) 686–691. `doi:10.1016/S0022-3115(06)80123-6`.

[25] V. Y. Sergeev, B. V. Kuteev, A. S. Bykov, S. V. Krylov, V. G. Skokov, V. M. Timokhin, Lithium technologies for edge plasma control, Fusion Engineering and Design 87 (10) (2012) 1765–1769. `doi:10.1016/j.fusengdes.2011.10.008`.

[26] A. Bortolon, V. Rohde, R. Maingi, E. Wolfrum, R. Dux, A. Herrmann, R. Lunsford, R. M. McDermott, A. Nagy, A. Kallenbach, D. K. Mansfield, R. Nazikian, R. Neu, ASDEX Upgrade Team, Real-time wall conditioning by controlled injection of boron and boron nitride powder in full tungsten wall ASDEX Upgrade, Nuclear Materials and Energy 19 (2019) 384 – 389. `doi:10.1016/j.nme.2019.03.022`.

[27] A. Bortolon, R. Maingi, A. Nagy, J. Ren, J. Duran, A. Maan, D. Donovan, J. Boedo, D. Rudakov, A. Hyatt, T. Wilks, M. Shafer, C. Samuell, M. Fenstermacher, E. Gilson, R. Lunsford, D. Mansfield, T. Abrams, R. Nazikian, Observations of wall conditioning by means of boron powder injection in DIII-D H-mode plasmas, Nuclear Fusion 60 (12) (2020) 126010. `doi:10.1088/1741-4326/abaf31`.

[28] E. Gilson, H. Lee, A. Bortolon, W. Choe, A. Diallo, S. Hong, H. Lee, J. Lee, R. Maingi, D. Mansfield, A. Nagy, S. Park, I. Song, J. Song, S. Yun, S. Yoon, R. Nazikian, Wall conditioning and ELM mitigation with boron nitride powder injection in KSTAR, Nuclear Materials and Energy 28 (2021) 101043. `doi:10.1016/j.nme.2021.101043`.

[29] Z. Sun, R. Maingi, J. Hu, W. Xu, G. Zuo, Y. Yu, C. Wu, M. Huang, X. Meng, L. Zhang,

L. Wang, S. Mao, F. Ding, D. Mansfield, J. Canik, R. Lunsford, A. Bortolon, X. Gong, EAST Team, Real time wall conditioning with lithium powder injection in long pulse H-mode plasmas in EAST with tungsten divertor, Nuclear Materials and Energy 19 (2019) 124–130. `doi:10.1016/j.nme.2019.02.029`.

[30] R. Maingi, J. S. Hu, Z. Sun, K. Tritz, G. Z. Zuo, W. Xu, M. Huang, X. C. Meng, J. M. Canik, A. Diallo, R. Lunsford, D. K. Mansfield, T. H. Osborne, X. Z. Gong, Y. F. Wang, Y. Y. Li, EAST Team, ELM elimination with Li powder injection in EAST discharges using the tungsten upper divertor, Nuclear Fusion 58 (2) (2018) 024003, publisher: IOP Publishing. `doi:10.1088/1741-4326/aa9e3f`.

[31] Z. Sun, A. Diallo, R. Maingi, Y. Qian, K. Tritz, Y. Wang, Y. Wang, A. Bortolon, A. Nagy, L. Zhang, Y. Duan, Y. Ye, H. Zhao, H. Wang, X. Gu, G. Zuo, W. Xu, M. Huang, C. Li, X. Meng, C. Zhou, H. Liu, Q. Zang, L. Wang, J. Qian, G. Xu, X. Gong, J. Hu, EAST Team, Suppression of edge localized modes with real-time boron injection using the tungsten divertor in EAST, Nucl. Fusion 61 (1) (2021) 014002. `doi:10.1088/1741-4326/abc763`.

[32] F. Nespoli, N. Ashikawa, E. Gilson, R. Lunsford, S. Masuzaki, M. Shoji, T. Oishi, C. Suzuki, A. Nagy, A. Mollen, N. Pablant, K. Ida, M. Yoshinuma, N. Tamura, D. Gates, T. Morisaki, LHD experiment group, First impurity powder injection experiments in LHD, Nuclear Materials and Energy 25 (2020) 100842. `doi:10.1016/j.nme.2020.100842`.

[33] R. Lunsford, C. Killer, A. Nagy, D. A. Gates, T. Klinger, A. Dinklage, G. Satheeswaran, G. Kocsis, S. A. Lazerson, F. Nespoli, N. A. Pablant, A. von Stechow, A. Alonso, T. Andreeva, M. Beurskens, C. Biedermann, S. Brezinsek, K. J. Brunner, B. Buttenschön, D. Carralero, G. Cseh, P. Drewelow, F. Effenberg, T. Estrada, O. P. Ford, O. Grulke, U. Hergenhahn, U. Höfel, J. Knauer, M. Krause, M. Krychowiak, S. Kwak, A. Langenberg, U. Neuner, D. Nicolai, A. Pavone, A. Puig Sitjes, K. Rahbarnia, J. Schilling, J. Svensson, T. Szepesi, H. Thomsen, T. Wauters, T. Windisch, V. Winters, D. Zhang, L. Zsuga, W7-X Team, Characterization of injection and confinement improvement through impurity induced profile modifications on the Wendelstein 7-X stellarator, Physics of Plasmas 28 (8) (2021) 082506. `doi:10.1063/5.0047274`.

[34] P. C. Stangeby, E. A. Unterberg, J. W. Davis, T. Abrams, A. Bortolon, I. Bykov, D. Donovan, H. Y. Guo, R. Kolasinski, A. W. Leonard, J. H. Nichols, D. L. Rudakov, G. Sinclair, D. M. Thomas, J. G. Watkins, Developing solid-surface plasma facing components for pilot plants and reactors with replenishable wall claddings and continuous surface conditioning. part a: concepts and questions, Plasma Physics and Controlled Fusion 64 (5) (2022) 055018. `doi:10.1088/1361-6587/ac5a7c`.

[35] T. Abrams, R. Ding, H. Guo, D. Thomas, C. Chrobak, D. Rudakov, A. McLean, E. Unterberg, A. Briesemeister, P. Stangeby, J. Elder, W. Wampler, J. Watkins, The inter-ELM tungsten erosion profile in DIII-D H-mode discharges and benchmarking with ERO+OEDGE modeling, Nuclear Fusion 57 (5) (2017) 056034. `doi:10.1088/1741-4326/aa66b2`.

[36] M. E. Fenstermacher, W. H. Meyer, R. D. Wood, D. G. Nilson, R. Ellis, N. H. Brooks, A tangentially viewing visible TV system for the DIII-D divertor, Review of Scientific Instruments 68 (1) (1997) 974–977. `doi:10.1063/1.1147729`.

[37] N. H. Brooks, A. Howald, K. Klepper, P. West, Multichord spectroscopy of the DIII-D divertor region, Review of Scientific Instruments 63 (10) (1992) 5167–5169. `doi:10.1063/1.1143469`.

[38] T. Morisaki, S. Masuzaki, M. Kobayashi, M. Shoji, J. Miyazawa, R. Sakamoto, G. Motojima, M. Goto, H. Funaba, H. Tanaka, K. Tanaka, I. Yamada, S. Ohdachi, H. Yamada, A. Komori, LHD Experiment Group, Initial experiments towards edge plasma control with a closed helical divertor in LHD, Nuclear Fusion 53 (6) (2013) 063014. `doi:10.1088/0029-5515/53/6/063014`.

[39] H. Guo, H. Wang, J. Watkins, L. Casali, B. Covele, A. Moser, T. Osborne, C. Samuell, M. Shafer, P. Stangeby, D. Thomas, J. Boedo, R. Buttery, R. Groebner, D. Hill, L. Holland, A. Hyatt, A. Jaervinen, A. Kellman, L. Lao, C. Lasnier, A. Leonard, C. Murphy, J. Ren, C. Sang, A. Sontag, T. Taylor, the DIII-D Team, First experimental tests of a new small angle slot divertor on DIII-D, Nucl. Fusion 59 (8) (2019) 086054. `doi:10.1088/1741-4326/ab26ee`.

[40] M. Shafer, B. Covele, J. Canik, L. Casali, H. Guo, A. Leonard, J. Lore, A. McLean, A. Moser, P. Stangeby, D. Taussig, H. Wang, J. Watkins, Dependence of neutral pressure on detachment in the small angle slot divertor at DIII-D, Nuclear Materials and Energy 19 (2019) 487–492. `doi:10.1016/j.nme.2019.04.003`.

[41] L. Casali, B. Covele, H. Guo, The effect of neutrals in the new SAS divertor at DIII-D as modelled by SOLPS, Nuclear Materials and Energy 19 (2019) 537–543. `doi:10.1016/j.nme.2019.03.021`.

[42] L. Casali, D. Eldon, A. McLean, T. Osborne, A. Leonard, B. Grierson, J. Ren, Impurity leakage and radiative cooling in the first nitrogen and neon seeding study in the closed DIII-D SAS

configuration, Nuclear Fusion 62 (2) (2022) 026021. `doi:10.1088/1741-4326/ac3e84`.

[43] O. Février, H. Reimerdes, C. Theiler, D. Brida, C. Colandrea, H. De Oliveira, B. Duval, D. Galassi, S. Gorno, S. Henderson, M. Komm, B. Labit, B. Linehan, L. Martinelli, A. Perek, H. Raj, U. Sheikh, C. Tsui, M. Wensing, Divertor closure effects on the TCV boundary plasma, Nuclear Materials and Energy 27 (2021) 100977. `doi:10.1016/j.nme.2021.100977`.

[44] A. Kallenbach, M. Balden, R. Dux, T. Eich, C. Giroud, A. Huber, G. Maddison, M. Mayer, K. McCormick, R. Neu, T. Petrie, T. Pütterich, J. Rapp, M. Reinke, K. Schmid, J. Schweinzer, S. Wolfe, ASDEX Upgrade Team, DIII-D Team, Alcator Team, JET-EFDA Contributors, Plasma surface interactions in impurity seeded plasmas, Journal of Nuclear Materials 415 (1, Supplement) (2011) S19–S26, proceedings of the 19th International Conference on Plasma-Surface Interactions in Controlled Fusion. `doi:10.1016/j.jnucmat.2010.11.105`.

[45] P. G. Carolan, V. A. Piotrowicz, The behaviour of impurities out of coronal equilibrium, Plasma Physics 25 (10) (1983) 1065–1086. `doi:10.1088/0032-1028/25/10/001`.

[46] H. P. Summers, N. R. Badnell, M. G. O'Mullane, A. D. Whiteford, R. Bingham, B. J. Kellett, J. Lang, K. H. Behringer, U. Fantz, K.-D. Zastrow, S. D. Loch, M. S. Pindzola, D. C. Griffin, C. P. Ballance, Atomic data for modelling fusion and astrophysical plasmas, Plasma Physics and Controlled Fusion 44 (12B) (2002) B323–B338. `doi:10.1088/0741-3335/44/12b/323`.

[47] A. Nagy, A. Bortolon, D. M. Mauzey, E. Wolfe, E. P. Gilson, R. Lunsford, R. Maingi, D. K. Mansfield, R. Nazikian, A. L. Roquemore, A multi-species powder dropper for magnetic fusion applications, Review of Scientific Instruments 89 (10) (2018) 10K121. `doi:10.1063/1.5039345`.

[48] W. W. Heidbrink, P. L. Taylor, J. A. Phillips, Measurements of the neutron source strength at DIII-D, Review of Scientific Instruments 68 (1) (1997) 536–539. `doi:10.1063/1.1147646`.

[49] T. Petrie, B. Grierson, T. Osborne, C. Petty, F. Turco, S. Allen, M. Fenstermacher, J. Ferron, H. Guo, E. Hinson, R. L. Haye, C. Lasnier, A. Leonard, A. McLean, B. Victor, H. Wang, J. Watkins, High performance double-null plasmas under radiating divertor and mantle scenarios on DIII-D, Nuclear Fusion 59 (8) (2019) 086053. `doi:10.1088/1741-4326/ab2936`.

[50] R. Lunsford, V. Rohde, A. Bortolon, R. Dux, A. Herrmann, A. Kallenbach, R. McDermott, P. David, A. Drenik, F. Laggner, R. Maingi, D. K. Mansfield, A. Nagy, R. Neu, E. Wolfrum, ASDEX Upgrade Team, Active conditioning of ASDEX upgrade tungsten plasma-facing components and discharge enhancement through boron and boron nitride particulate injection, Nuclear Fusion 59 (12) (2019) 126034. `doi:10.1088/1741-4326/ab4095`.

[51] K. Krieger, M. Balden, A. Bortolon, F. Laggner, V. Rohde, W. Wampler, ASDEX Upgrade Team, Boron redistribution after boron powder injection in ASDEX Upgrade, 2022, 25th International Conference on Plasma Surface Interactions 2022, 25th PSI.

[52] F. Effenberg, S. Abe, F. Laggner, D. Rudakov, G. Sinclair, W. W.R., T. Abrams, D. Mauzey, A. Nagy, F. Scotti, R. Nazikian, DIII-D Team, In-situ growth of silicon-rich layers with Si granule injection in DIII-D H-mode plasmas, 2022, 25th International Conference on Plasma Surface Interactions 2022, 25th PSI.

[53] T. Abrams, G. Sinclair, J. H. Nichols, E. A. Unterberg, D. C. Donovan, J. Duran, J. D. Elder, F. Glass, B. A. Grierson, H. Y. Guo, T. Hall, X. Ma, R. Maurizio, A. G. McLean, C. Murphy, R. Nguyen, D. L. Rudakov, P. C. Stangeby, D. M. Thomas, S. A. Zamperini, Design and physics basis for the upcoming DIII-D SAS-VW campaign to quantify tungsten leakage and transport in a new slot divertor geometry, Physica Scripta 96 (12) (2021) 124073. `doi:10.1088/1402-4896/ac3c5f`.

[54] W. Xu, J. S. Hu, Z. Sun, R. Maingi, L. Zhang, Y. W. Yu, C. L. Li, G. Z. Zuo, Y. Z. Qian, M. Huang, X. C. Meng, W. Gao, Y. M. Duan, Y. J. Chen, K. Wang, X. D. Lin, X. Gao, Effect of lithium coating on long pulse high performance plasma discharges in EAST, Plasma Physics and Controlled Fusion 62 (8) (2020) 085012. `doi:10.1088/1361-6587/ab9b3a`.

[55] M. S. Vorenkamp, A. Nagy, A. Bortolon, R. Lunsford, R. Maingi, D. K. Mansfield, A. L. Roquemore, Recent upgrades of the DIII-D impurity granule injector, Fusion Science and Technology 72 (3) (2017) 488–495. `doi:10.1080/15361055.2017.1335144`.

[56] A. Nagy, A. Bortolon, D. Gates, E. Gilson, C. Killer, T. Klinger, R. Lunsford, R. Maingi, D. Mansfield, D. Mauzey, R. Nazikian, L. Roquemore, E. Wolfe, A horizontal powder injector for W7-X, Fusion Engineering and Design 146 (2019) 1403–1407. `doi:10.1016/j.fusengdes.2018.12.099`.

[57] A. Bortolon, R. Maingi, D. Mansfield, A. Nagy, A. Roquemore, L. Baylor, N. Commaux, G. Jackson, E. Gilson, R. Lunsford, P. Parks, C. Chrystal, B. Grierson, R. Groebner, S. Haskey, M. Makowski, C. Lasnier, R. Nazikian, T. Osborne, D. Shiraki, M. V. Zeeland, High frequency pacing of edge localized modes by injection of lithium granules in DIII-D H-mode discharges, Nuclear Fusion 56 (5) (2016) 056008. `doi:10.1088/0029-5515/56/5/056008`.

[58] D. Orlov, Hypervelocity impact in stellar media: Spacecraft Heat Shield study in DIII-D*, in: APS Division of Plasma Physics Meeting Abstracts, Vol. 2021 of APS Meeting Abstracts, 2021, p. WI02.002.